

Moment-Based Method to Statistically Categorize Rock Outcrops Based on their Topographical Features

Roger C. Gauss, Joseph M. Fialkowski, David C. Calvo, and Richard Menis

Acoustics Division, Code 7160

Naval Research Laboratory

Washington, DC 20375-5350, USA

Derek R. Olson

Applied Research Laboratory, The Pennsylvania State University
State College, PA 16804-0030, USA

Anthony P. Lyons

Center for Coastal and Ocean Mapping
The University of New Hampshire
Durham, NH 03824, USA

Abstract—Geomorphological formations on the ocean seafloor are spatially complex objects. Rock outcrops in particular can be spatially compact, and highly anisotropic in their large- and small-scale topographic structure, and represent a significant source of clutter for short-range active sonars operating in shallow water. This paper describes a physical moment-based statistical method for categorizing rock outcrops based on their topographical characteristics, in particular isolating its facet-like features. The correspondence of these features to clutter-generating objects is then substantiated for a short-range, high-frequency shallow-water scenario, where the ensonified area is a fraction of outcrop size, via comparisons with high-fidelity acoustic backscattering predictions.

Keywords—seafloor features; outcrop; bathymetric facets; topography; PDF; non-Rayleigh; Poisson-Rayleigh; sonar clutter

I. INTRODUCTION

Glacially-eroded rock outcrops¹, such as *roches moutonnées* [1], on the ocean seafloor can be spatially complex objects: anisotropic and spatially compact, with sizes that range widely from less than a meter to hundreds of meters. They are formed through the two erosional processes of glacial quarrying, which produces stepped, faceted surface features, and glacial abrasion, which produces very smooth, gently undulating surface features [1]. Of particular interest to

mobile active sonars operating in shallow water are areas of outcrops oriented close to normal incidence to the sonar system, defined here as facets—as they can generate strong specular reflections, and so be a source of acoustic false targets [2]. While the term facets can refer to planar regions much larger than the acoustic wavelength, facets here will refer to near-normal-incidence areas. This paper introduces a moment-based statistical method for categorizing rock outcrops by their topographical features, with the focus on identifying facet-like features. As the acoustic significance of these reflectors depends not only on their slope characteristics but their relative surface heights/sizes [2]–[3], the method is designed to automatically incorporate both feature slope and height information².

II. MOMENT-BASED MODEL

The categorization method leverages the two-parameter Poisson-Rayleigh (P-R) probability density function (PDF) model [2], [6]. It models data amplitudes as a joint process arising from two statistically independent mechanisms, namely returns from a continuous background and a set of sizable/strong discrete events. Its key parameters are α which represents the effective number of discrete scatterers, and ρ_D^2 their relative strength:

$$\rho_c^2 + \alpha\rho_D^2 = 1. \quad (1)$$

¹These type of outcrops are common in areas of past glacial coverage (where they have not been buried by layers of sediment). Outcrops in general can be any type of rock, but *roches moutonnées* (sheepbacks) tend to be composed of harder material (intrusive igneous or metamorphic). Sedimentary or extrusive igneous rock (formed from lava rather than magma-like basalt) may result in different morphology.

²Other factors important to echo statistics such as propagation effects [4] and beampattern effects [5] are not considered here.

Work supported by the U.S. Office of Naval Research.

In (1), ρ_c^2 is proportional to the Rayleigh background power, and $\alpha\rho_d^2$ is proportional to the Rayleigh power associated with discrete scatterers. (In this normalized form of the P-R model [2], the Rayleigh power of the distribution has been factored out.)

Like the popular K-type model [7], the P-R model provides a physical context for relating the characteristics of data distributions to feature attributes. However, with its extra degree of freedom, the P-R model has a major advantage over conventional single-parameter models in being able to describe a wide range of data distributions, offering the potential to exploit more information through higher-order data moments, and thus do a better job of categorizing geospatial features.

Another advantage of the P-R model is that its parameters can be efficiently estimated (via closed-form equations) from data via the 2nd, 4th, and 6th moment equations of the P-R distribution. For each range/cross-range cell of fixed sample size N , the 4th and 6th normalized moments are first computed from the data r_i :

$$\eta_4 = \mu_4 / \mu_2^2 \quad , \quad \eta_6 = \mu_6 / \mu_2^3 \quad , \quad \text{where} \quad (2)$$

$$\mu_k = \frac{1}{N} \sum_{i=1}^N r_i^k .$$

Then the moments of (2) are used to form the P-R discrete-event parameters:

$$\alpha = \frac{9(\zeta\eta_4 - 2)^3}{2(\zeta^2\eta_6 - 9\zeta\eta_4 + 12)^2} \quad , \quad \rho_d^2 = \frac{(\zeta^2\eta_6 - 9\zeta\eta_4 + 12)}{3(\zeta\eta_4 - 2)} . \quad (3)$$

In (3), the constant $\zeta \geq 1$ is added to translate the discrete density and strength parameter estimates in order to ensure that they are valid in the context of the P-R model. This is equivalent to zero-filling the data window over which the normalized moments of (2) are computed, where $\zeta - 1$ gives the ratio of zero to non-zero data points. While the above results are inherently biased, they nevertheless provide a valid relative measure of the properties of discrete scatterers, and therefore are potentially useful as categorization clues. (For this data set, ζ was set to 50.)

To further isolate facet-like features of sufficient size from other strong scatterers, we define a single P-R-based

parameter β that exploits strength, density and clutter characteristics:

$$\beta = 10^\chi, \quad \chi = \log_{10}(\rho_d^2) - |\log_{10}(\alpha\rho_d^2)| . \quad (4)$$

This P-R combination parameter β emphasizes data exhibiting a dominant discrete scatterer component as typified by larger values of ρ_d^2 and proximity to unit discrete power $\alpha\rho_d^2$. It was found that this parameter was more robust than either α or ρ_d^2 in isolating potential false targets.

III. OUTCROP DATA

The rock-outcrop bathymetric data used in this paper were obtained by the Norwegian Defence Research Establishment (FFI) off the coast of Larvik, Norway in April, 2011 [8] using their HUGIN 1000 HUS AUV equipped with a dual 100-kHz HISAS 1030 interferometric synthetic aperture sonar (SAS) for high-resolution bathymetry estimation [9]. The bathymetric resolution was ~ 0.18 m in the horizontal and $\sim 0.1\text{--}0.15$ m in the vertical.

Fig. 1 displays a sonar image of the rock outcrop (*roche moutonnée* [1]) studied in this paper. Note that the outcrop contains both glacially abraded and quarried portions.

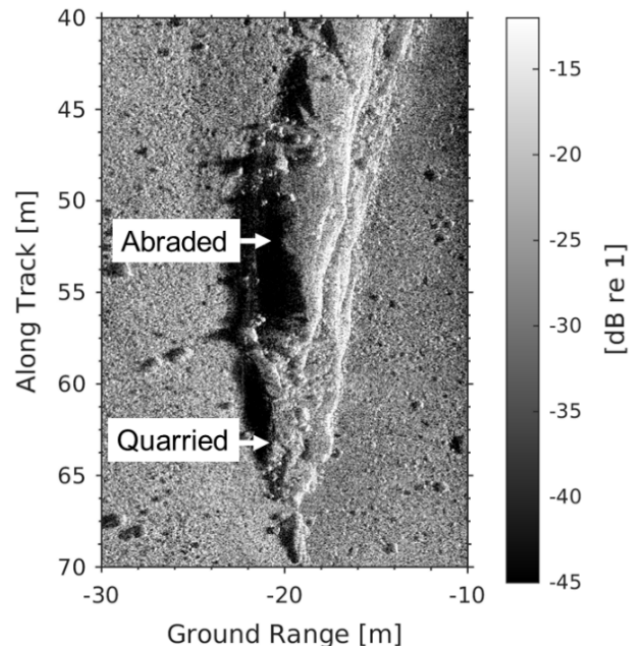


Fig. 1. SAS complex imagery of rock outcrop (courtesy of FFI). (The image resolution is $\sim 0.03 \times 0.03$ m.)

IV. STATISTICAL BATHYMETRIC FEATURE CHARACTERIZATION

As noted previously, facet-like features of outcrops with sufficient size and slope are potential sonar clutter objects, and are the focus of this paper. Fig. 2a shows the elevation data for the part of the rock outcrop on which we concentrated our analysis. These bathymetric data were 2-D linearly interpolated in some patch areas by the authors in cases where sufficiently-high coherence data were not available. Fig. 2b shows the corresponding bathymetric slope distribution, where for each pixel the maximum slope over all directions is displayed.

The next step is to characterize the outcrop via its spatial statistics. To illustrate the potential of the P-R model to categorize bathymetric features, Fig. 3a shows an example where a window of $\sim 0.4 \times 0.4$ m slides over a track traversing part of the outcrop, while Fig. 3b displays the resultant sampled bathymetric data (open circles) and example P-R model values (red curves). While commonly-used models like the K-distribution can match PDF tails, Fig. 3b shows the potential of our 2-parameter P-R model to categorize bathymetric features by matching data-distribution shape as

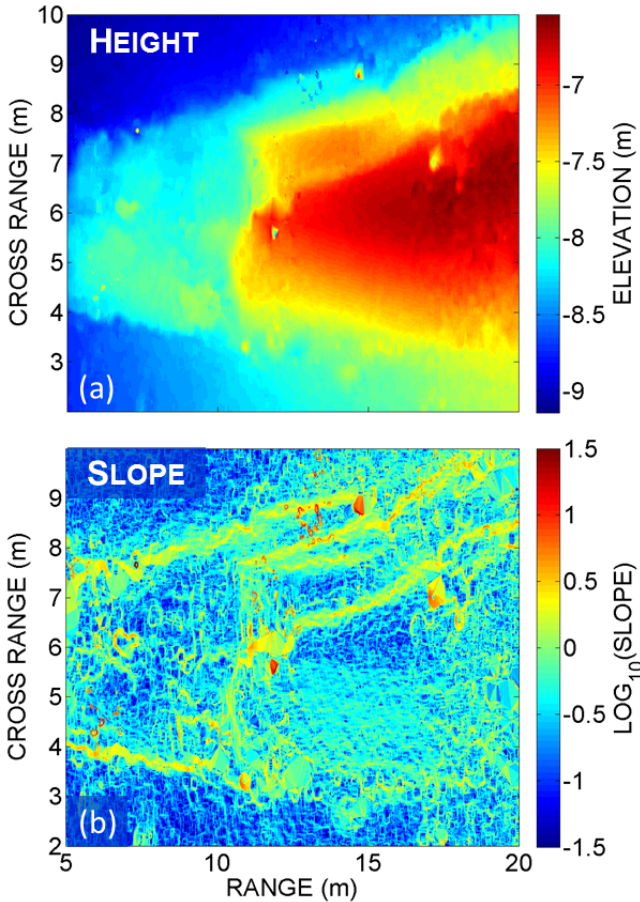


Fig. 2. (a) High-resolution rock-outcrop elevation data and (b) corresponding maximum local slope at each pixel. (Note the cross-range (ground-range) orientation is flipped from that of Fig. 1.)

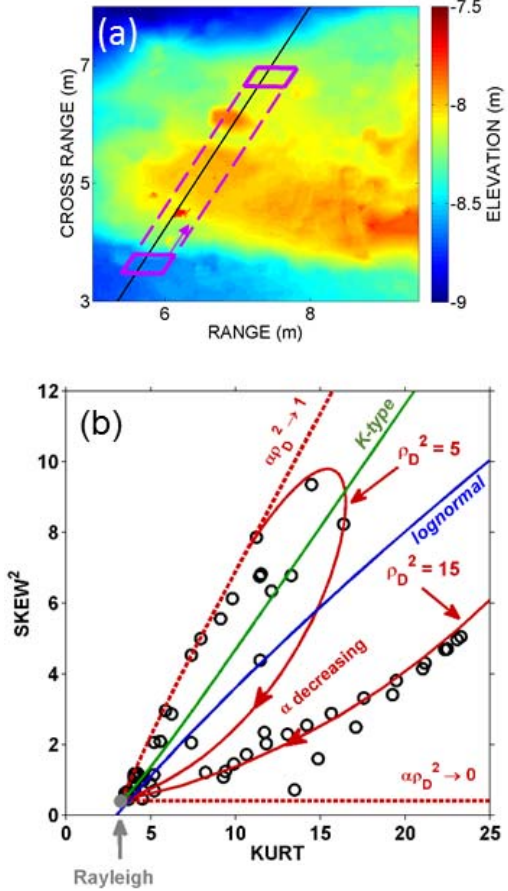


Fig. 3. (a) High-resolution bathymetric data and (b) corresponding average skewness²-kurtosis values (symbols) computed in sliding windows (magenta boxes in (a) in 0.4-m range steps), overlain with PDF model curves.

measured via higher-order statistical moments³. While the non-acoustic data do not strictly satisfy the underlying model assumptions, the physical context of the model parameters can still provide a useful tool for categorizing bathymetric features.

In general, the outcrop's bathymetric features relevant to the short-range sonar problem fell into two broad categories, representing those that are very compact and those of more moderate size. Fig. 3b shows that a significant number of feature statistics lie along a curve corresponding to a large constant P-R discrete-strength parameter value ($\rho_D^2 = 15$) with smaller density parameter values. These data indicate bathymetric features which while spatially isolated and large relative to the local neighborhood, are acoustically small and generally not likely to possess significant scattering components. Conversely, several feature statistics lie along the curve corresponding to a smaller constant discrete strength

³How PDF models depend on skewness and kurtosis illustrate their generality or narrowness in representing higher-order moments, and so matching data [10].

($\rho_D^2 = 5$) and larger density values. These data indicate bathymetric features which statistically appear as clusters of objects and while having lower relative strength, are moderately sized, suggesting that they could be acoustically noteworthy scattering objects—in particular, those P-R-derived values near the intersection of the $\alpha\rho_D^2 = 1$ line and the $\rho_D^2 = 5$ curve.

V. CLUTTER CHARACTERIZATION

To explore automatically identifying the discrete ‘clutter-like’ features of interest, a set of moment-based statistical models were applied to the height-distribution data. The domain was gridded into 0.5×0.5 m cells centered on each pixel, and ensemble statistics generated for each cell⁴. Fig. 4 shows two such statistics, the P-R-based β and skewness. (Skewness captured more features than kurtosis.) In this case, β was estimated via (2)–(4) producing a biased result whereby prominent scattering features are associated with

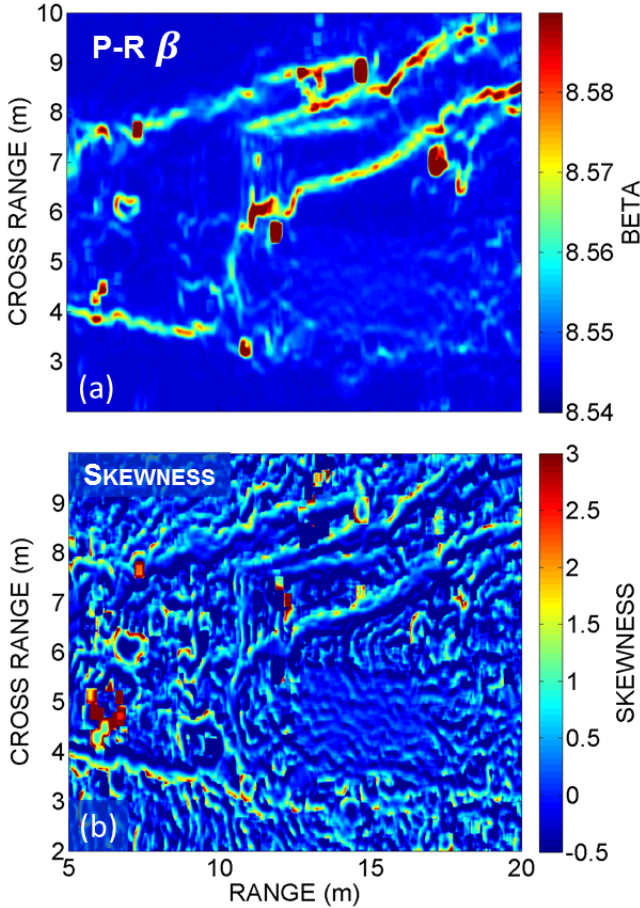


Fig. 4. Ensemble statistics of high-resolution rock-outcrop elevation data in 0.5-by-0.5-m cells: (a) P-R-based β and (b) skewness.

⁴For this data set, different cell sizes were investigated, with 0.5 m providing a good trade-off between spatial resolution and statistical estimation stability.

larger values of ρ_D^2 and values of discrete power $\alpha\rho_D^2$ close to, but greater than 1. The linear features prominent in Fig. 4a correspond to the abraded portions of the outcrop (cf. Fig. 1). Both the abraded and the quarried portions of the outcrop also exhibit more localized (‘point-like’) features as well.

Note how, in contrast to skewness, the P-R-based β picks up the leading edges of the bathymetric features exhibiting slope, with its value scaled to their relative prominence (cf. Fig. 2b). (The leading edges of topographical features are typically prime sonar clutter sources [2].)

Fig. 5a shows a 2D example of how the combination P-R parameter value corresponds to the local bathymetry as a function of range. It shows the potential of a physical moment-based model to automatically capture the salient geophysical spatial structure (such as local slope).

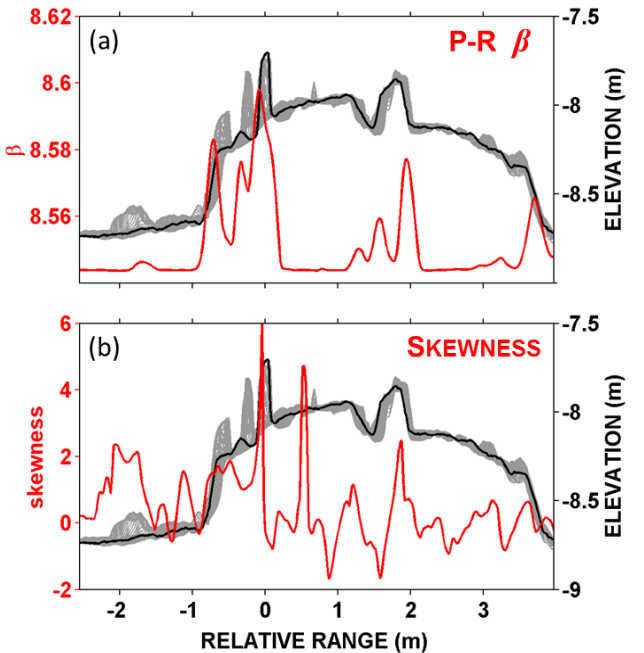


Fig. 5. Ensemble statistics (red curves) of (a) P-R-based β and (b) skewness extracted from 0.5-m cells (Fig. 4) centered along a line corresponding to the black line in Fig. 3a—the heavy black curve is the bathymetry along the black line, and the gray curves are the bathymetry along parallel adjacent lines (within the full parallelogram of Fig. 3a).

To substantiate this P-R-based morphological categorization with the acoustics, full-wave simulations and tank measurements of high-resolution backscattering from the outcrop have been conducted using deterministic numerical and physical scale models [11], respectively. A finite-element method (FEM/COMSOL Multiphysics) was used in a 2D (range/depth geometry) to model coherent acoustic elastic backscattering from the given bathymetric profiles. Both impenetrable (rigid) and penetrable monzonite [12] acoustic bottoms were examined.

Fig. 6 provides ‘direct-path’ monostatic geometry examples (in the same vertical plane as that of the heavy black line in Fig. 5, and the black line in Fig. 3a) showing the backscattered field for three ensonification angles created by a 15-kHz piston transducer (0.46-m diameter with a beam half angle of $\sim 5^\circ$) at an effective ‘far-field’ distance of 10 m. (Downrange high-frequency active sonar resolutions can be $O(0.1\text{m})$, so a fraction of outcrop size.) This plot shows that the scattering is complex due to the interaction of the beam footprint with the (rigid) multi-faceted surface, with visible shadowing and specular scattering notable at particular ranges. (Scattering levels are relative to source pressure levels.) Strong scattering from the moderately-sized, but facet-like (relatively-high-slope) features are evident. As expected, backscattering levels are variable with ensonification angle. In general, for a given ping, intensity variations will be due to a combination of sonar characteristics (spatial resolution, steering angle, geometry, etc.) and environmental variations (seafloor, oceanography, etc.).

Systematic application of full-wave modeling (varying sonar and environmental parameters) and tank-measurement data are being used to refine the clutter-model parameters, and determine sensitivity to sonar parameters (such as steering angle, beamwidth, and signal bandwidth).

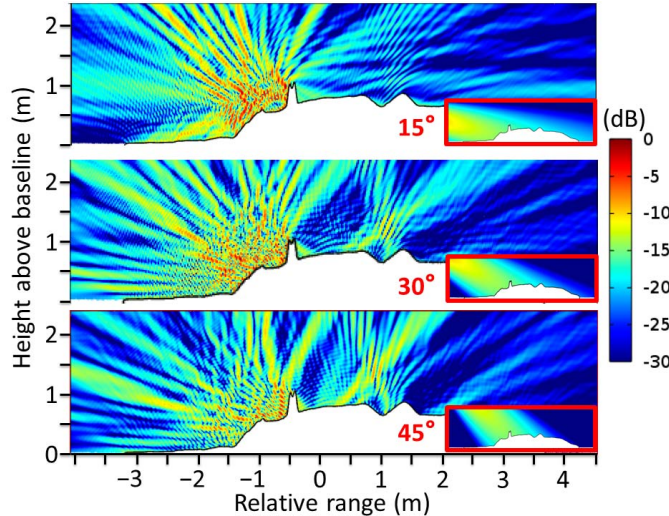


Fig. 6. Simulated 2-D coherent direct-path ensonification of the rock outcrop at 15 kHz by an effective-10-m-distant source-receiver (in the same vertical plane as the heavy black line of Fig. 5, and the black line of Fig. 3a). The backscattered field (pressure squared) is shown for 3 incident grazing angles of 15° , 30° and 45° . For each case, the inset in the red box displays the incident acoustic field.

VI. DISCUSSION

While this limited study was done on a single outcrop, the results suggest that given a sufficiently high-resolution bathymetric database, a P-R-model-based parameterization offers potential for helping to automatically identify the topographical feature information (local size, slope) that are of

most import acoustically. While mobile highly-directional sonars following a track will not always see a strong echo from a given feature because of the relative facet orientation or the sonar steering angle, the method nevertheless can help identify those objects as clutter when a threshold exceedance is encountered, or identify in advance potential clutter objects if a high-resolution bathymetric database is available. Furthermore, the results suggest that the P-R model can enhance the fidelity of sonar simulators by providing a computationally-fast, physical model for estimating the probability of false alarm (PFA) due to outcrops.

ACKNOWLEDGMENT

The authors would like to thank the Norwegian Defence Research Establishment (FFI), in conjunction with the Applied Research Laboratory/Pennsylvania State University, for providing the bathymetric rock-outcrop data, and in particular Torstein O. Sæbø and Roy E. Hansen of FFI.

REFERENCES

- [1] M. Bennet and N. Glasser, *Glacial Geology: Ice Sheets and Landforms*, 2nd ed., Wiley-Blackwell: Chichester, UK, 2009, ch. 5.
- [2] J. Fialkowski and R. Gauss, “Methods for identifying and controlling sonar clutter,” *IEEE J. Ocean. Eng.*, vol. 35, no. 2, pp. 330-354, Apr. 2010.
- [3] K. Becker, “Effect of various surface-height-distribution properties on acoustic backscattering statistics,” *IEEE J. Ocean. Eng.*, vol. 29, no. 2, pp. 246-259, Apr. 2004.
- [4] M. Trevorrow, “Statistics of fluctuations in high-frequency low-grazing-angle backscatter from a rocky sea bed,” *IEEE J. Ocean. Eng.*, vol. 29, no. 2, pp. 236-245, Apr. 2004.
- [5] D. Chu and T. Stanton, “Statistics of echoes from a directional sonar beam insonifying finite numbers of single scatterers and patches of scatterers,” *IEEE J. Ocean. Eng.*, vol. 35, no. 2, pp. 267-277, Apr. 2010.
- [6] J. Fialkowski, R. Gauss and D. Drumheller, “Measurements and modeling of low-frequency near-surface scattering statistics,” *IEEE J. Ocean. Eng.*, vol. 29, no. 2, pp. 197-214, Apr. 2004.
- [7] A. Lyons and D. Abraham, “Statistical characterization of high-frequency shallow-water seafloor backscatter,” *J. Acoust. Soc. Am.*, vol. 106, no. 3, pp. 1307-1315, 1999.
- [8] Ø. Midtgård, R. Hansen, T. Sæbø, V. Myers, J. Dubberley, and I. Quidu, “Change detection using synthetic aperture sonar: Preliminary results from the Larvik trial,” in Proc. MTS/IEEE OCEANS Conf., Kona, HI, 2011.
- [9] T. Fossum, T. Sæbø, B. Langli, H. Callow, and R. Hansen, “HISAS 1030 – High-resolution interferometric synthetic aperture sonar,” in Proc. Can. Hydrol. Conf., Victoria, BC, Canada, May 2008.
- [10] D. Abraham, “Modeling non-Rayleigh reverberation,” NATO SACLANT Undersea Res. Cntr., La Spezia, Italy, SACLANT Undersea Res. Cntr. Rep. SR-266, Jun. 1997.
- [11] D. Calvo, M. Nicholas, J. Fialkowski, R. Gauss, D. Olson, and A. Lyons, “Scale-model scattering using 3D printed representations of ocean bottom features,” in Proc. MTS/IEEE OCEANS’15 Conf. Washington, National Harbor, MD, 2015.
- [12] E.-R. Neumann, “Petrogenesis of the Oslo region Larvikites and associated rocks,” *J. Petrol.*, vol. 21, no. 3, pp. 499-531, Aug. 1980.